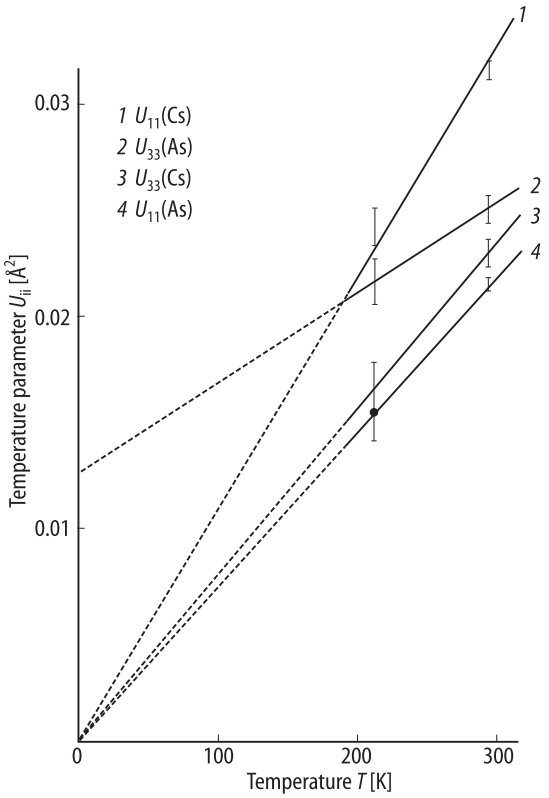

Fig. 33A-9-001. CsD_2AsO_4 (DCDA). U_{ii} vs. T [81Hay]. U_{ii}: temperature parameters defined by Eq. (d) in Introduction.

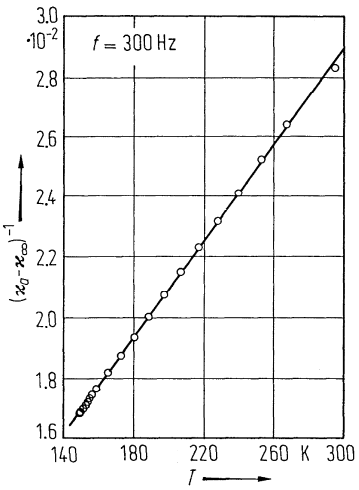

Fig. 33A-9-002. CsH_2AsO_4 (CDA). $(\kappa_a - \kappa_\infty)^{-1}$ vs. T [75Pol]. $\kappa_\infty = 15.3$.

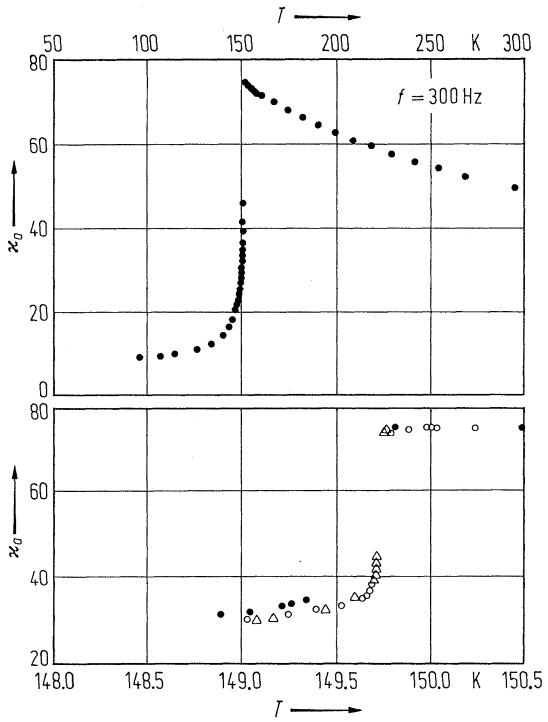

Fig. 33A-9-003. CsH_2AsO_4 (CDA). κ_a vs. T [75Pol]. The lower figure shows the behavior in the vicinity of Θ_f (open and full circles: cooling, triangles: heating).

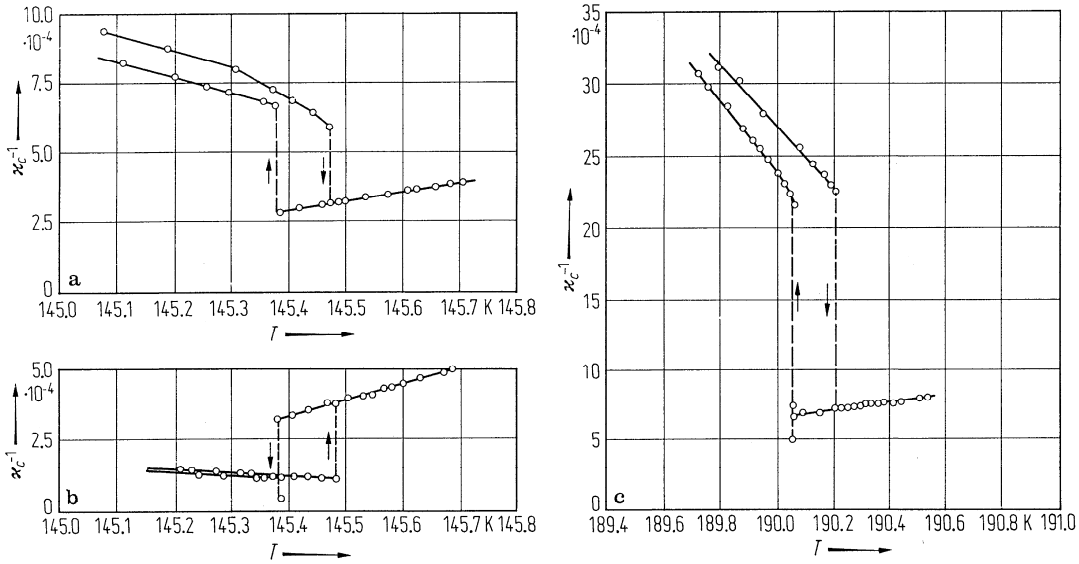

Fig. 33A-9-004. CsH_2AsO_4 (CDA), CsD_2AsO_4 (DCDA). κ_c^{-1} vs. T in the vicinity of Θ_f [73Str]. (**a**) CDA aged sample. (**b**) CDA fresh sample. (**c**) DCDA.

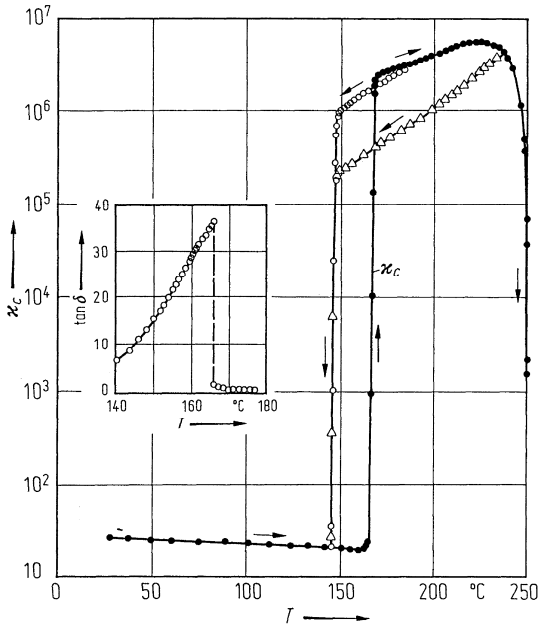

Fig. 33A-9-005. CsH_2AsO_4 (CDA). $\varkappa_c$, tan δ vs. T [77Gof]. f = 1 kHz.

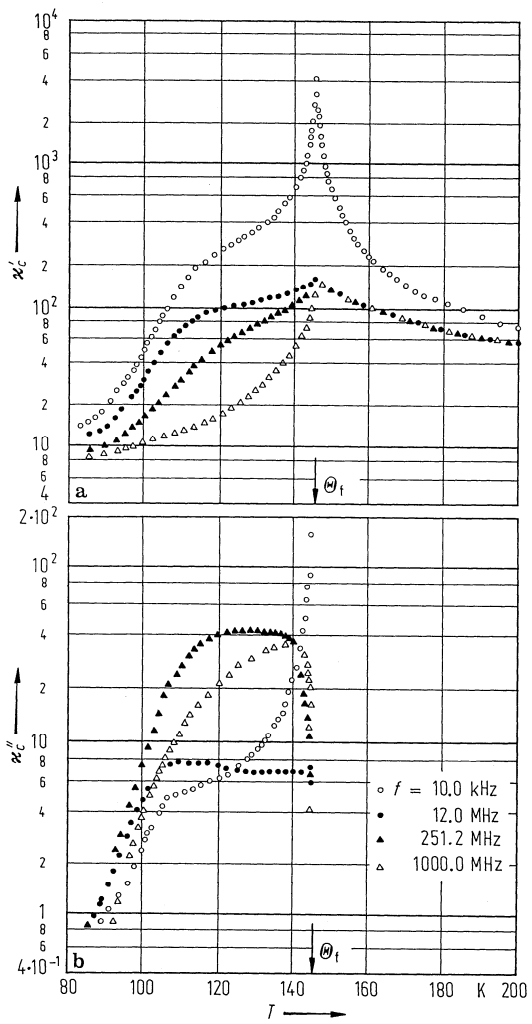

Fig. 33A-9-006. CsH_2AsO_4 (CDA). (**a**) κ'_c, (**b**) κ''_c vs. T [88Hay]. Parameter: f.

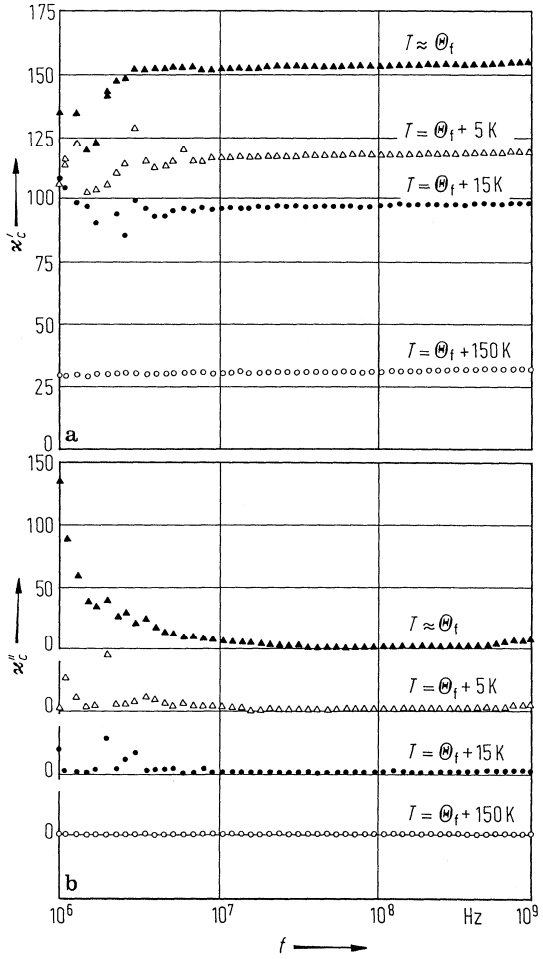

Fig. 33A-9-007. CsH_2AsO_4 (CDA). (**a**) κ'_c, (**b**) κ''_c vs. f above Θ_f [88Hay]. Parameter: T.

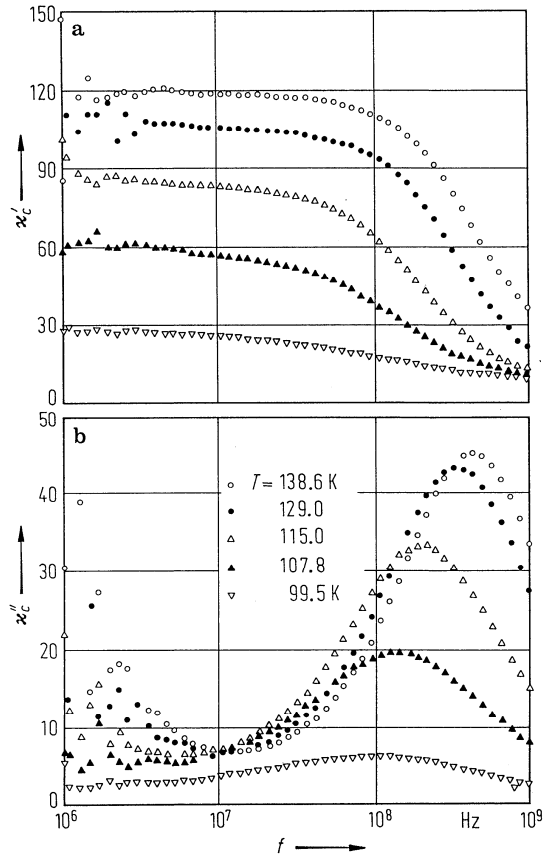

Fig. 33A-9-008. CsH_2AsO_4 (CDA). (**a**) κ_c', (**b**) κ_c'' vs. f below Θ_f [88Hay]. Parameter: T.

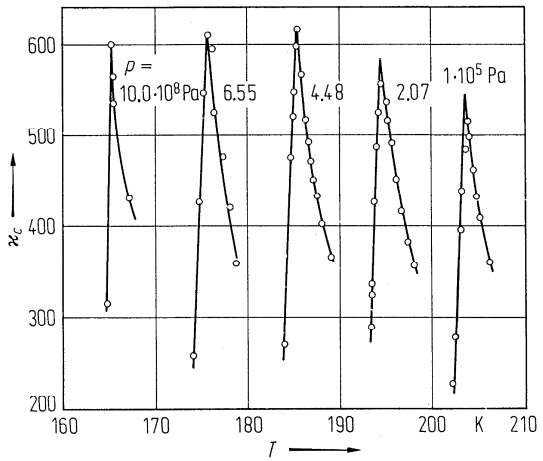

Fig. 33A-9-009. CsD_2AsO_4 (DCDA). κ_c vs. T [75Low]. Parameter: p. f = 1...100 kHz.

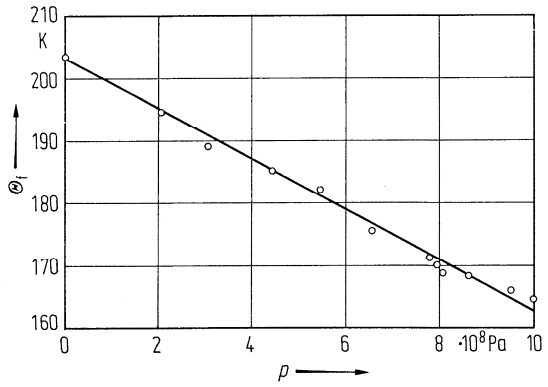

Fig. 33A-9-010. CsD_2AsO_4 (DCDA). Θ_t vs. p [75Low].

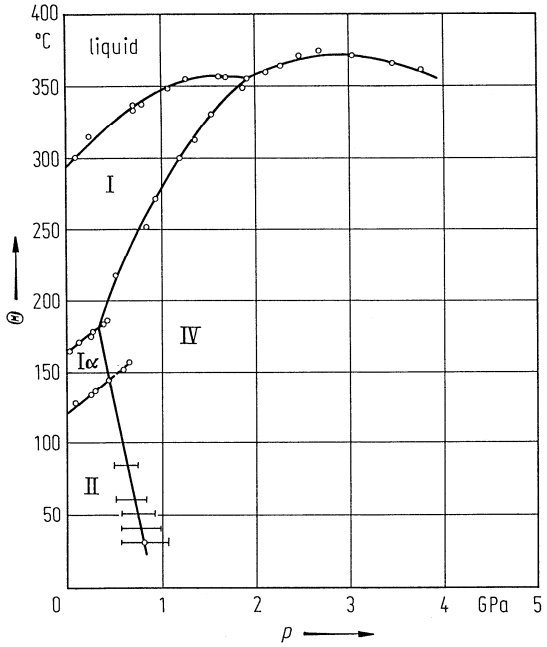

Fig. 33A-9-011. CsH_2AsO_4 (CDA). Θ vs. p [81Har].

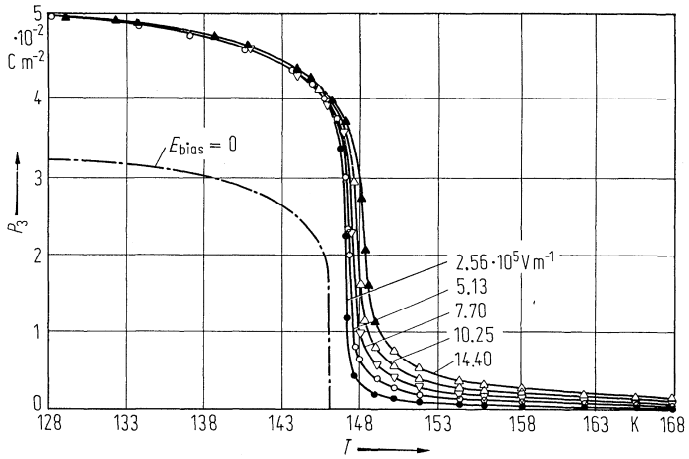

Fig. 33A-9-012. CsH_2AsO_4 (CDA). P_3 vs. T [75Cha]. Parameter: E_{bias}.

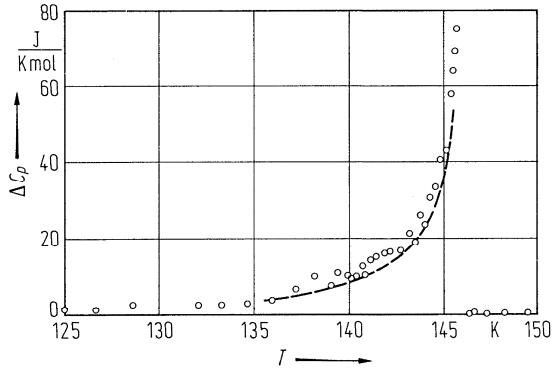

Fig. 33A-9-013. CsH_2AsO_4 (CDA). ΔC_p vs. T [74Deu]. ΔC_p: anomalous part of the molar heat capacity at constant pressure. Dashed line: calculated values.

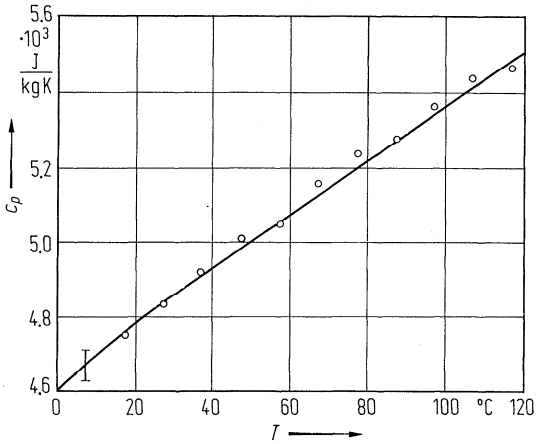

Fig. 33A-9-014. CsD_2AsO_4 (DCDA). c_p vs. T [75Liu]. c_p: specific heat capacity at constant pressure.

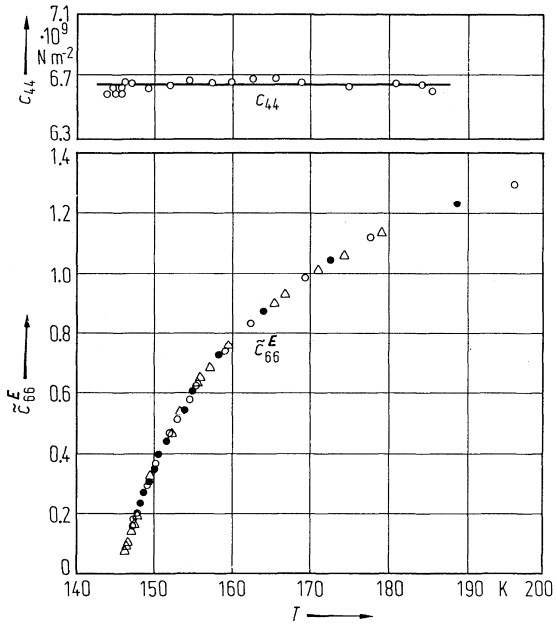

Fig. 33A-9-015. CsH_2AsO_4 (CDA). $c_{44}, \tilde{c}^{E}_{66}$ vs. T [75Pol]. $\tilde{c}^{E}_{66} \equiv c^{E}_{66}(T) / c^{E}_{66}$ (170 K). Open circles: 5 MHz, full circles: 10 MHz, triangles: 0.75...3 MHz.

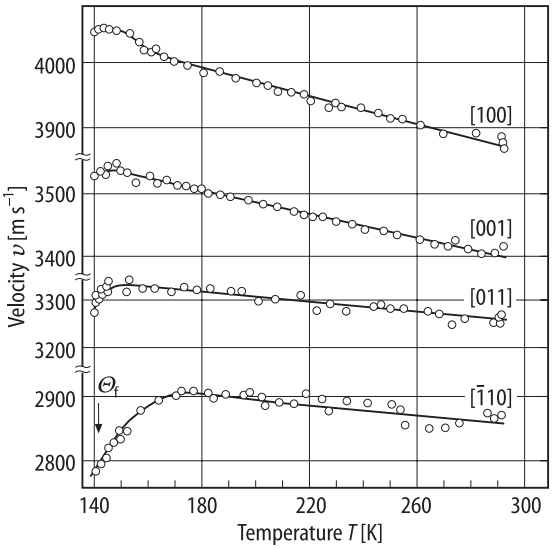

Fig. 33A-9-016. CsH_2AsO_4 (CDA). v vs. T [89Str]. v: longitudinal ultrasonic wave velocity. f = 10 MHz. Directions of the wave propagation are indicated.

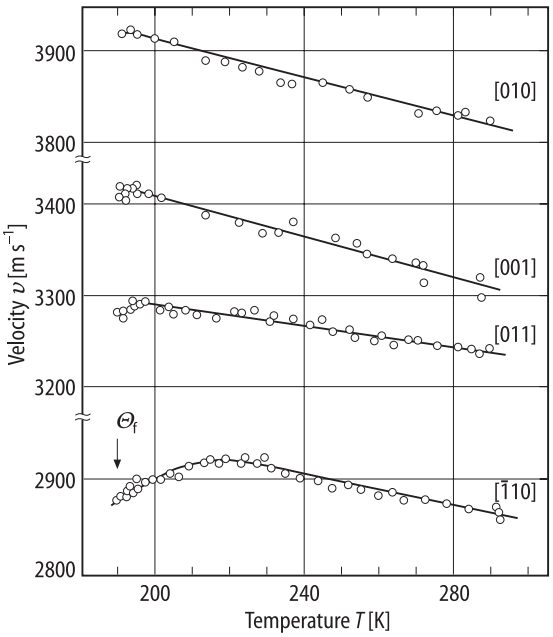

Fig. 33A-9-017. CsD_2AsO_4 (DCDA). v vs. T [89Str]. v: longitudinal ultrasonic wave velocity. f = 10 MHz. Directions of the wave propagation are indicated.

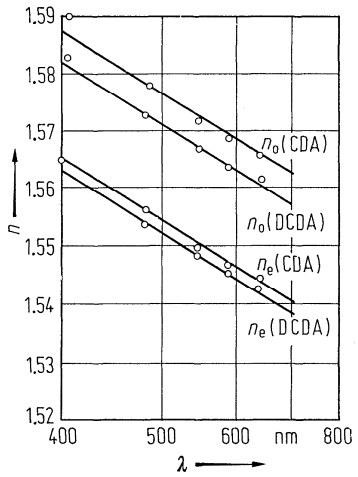

Fig. 33A-9-018. CsH_2AsO_4 (CDA), CsD_2AsO_4 (DCDA). n vs. λ at RT [69Adh].

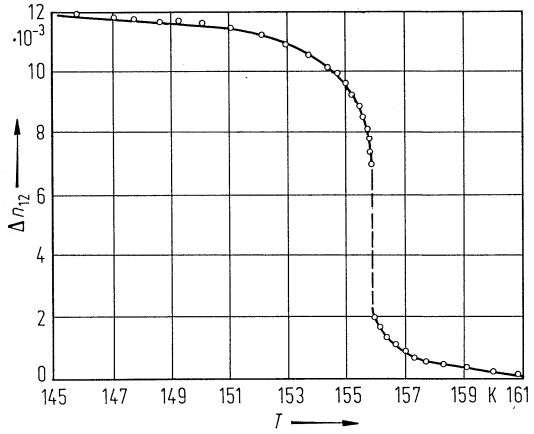

Fig. 33A-9-019. CsH_2AsO_4 (CDA). Δn_{12} vs. T [80Ani]. $\lambda = 632.8$ nm.

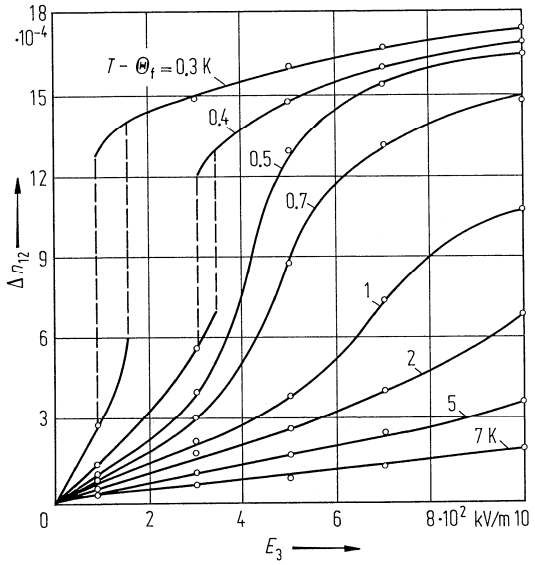

Fig. 33A-9-020. CsH_2AsO_4 (CDA). Δn_{12} vs. E_3 [80Ani]. Parameter: $T - \Theta_f$. $\lambda = 632.8$ nm.

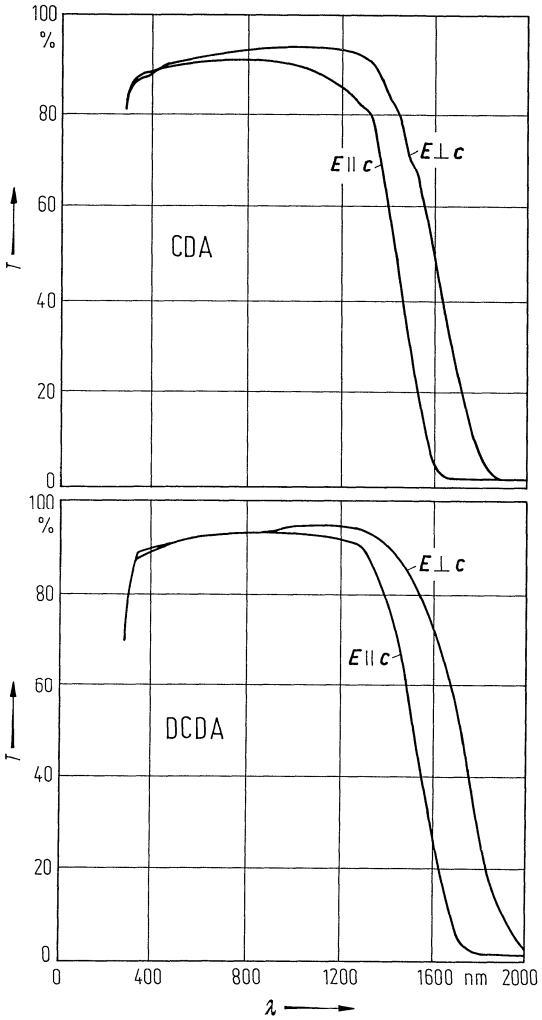

Fig. 33A-9-021. CsH_2AsO_4 (CDA), CsD_2AsO_4 (DCDA). *T* vs. λ [87Eim]. *T*: transmission. Sample thickness: 11 mm.

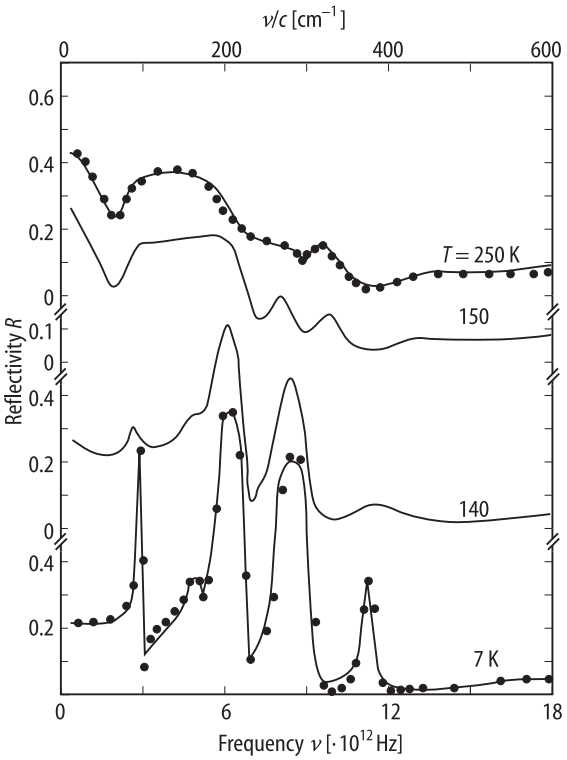

Fig. 33A-9-022. CsH_2AsO_4 (CDA). R vs. ν [93Wyn]. R: infrared reflectivity. Parameter: T. $\boldsymbol{E} \parallel \boldsymbol{c}$. Dots represent the best fit of the data with the factorized form of dielectric function.

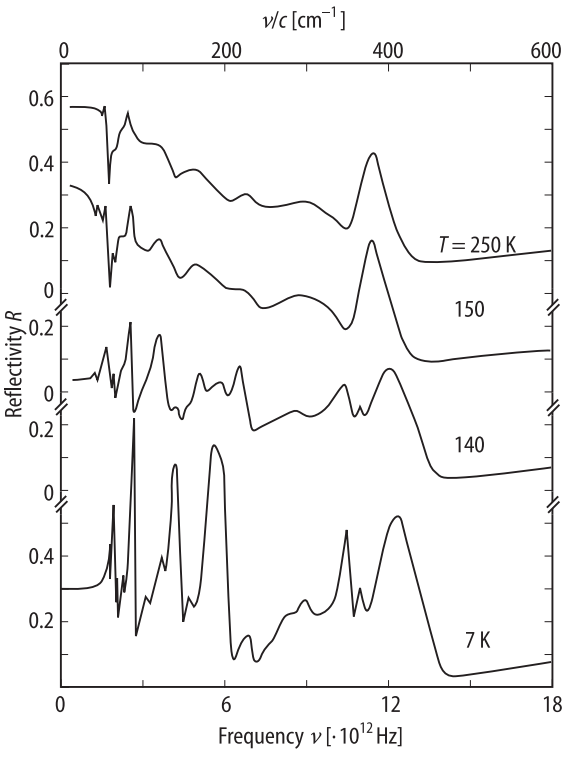

Fig. 33A-9-023. CsH_2AsO_4 (CDA). R vs. ν [93Wyn]. R: infrared reflectivity. Parameter: T. $\boldsymbol{E} \perp \boldsymbol{c}$ in (100) plane.

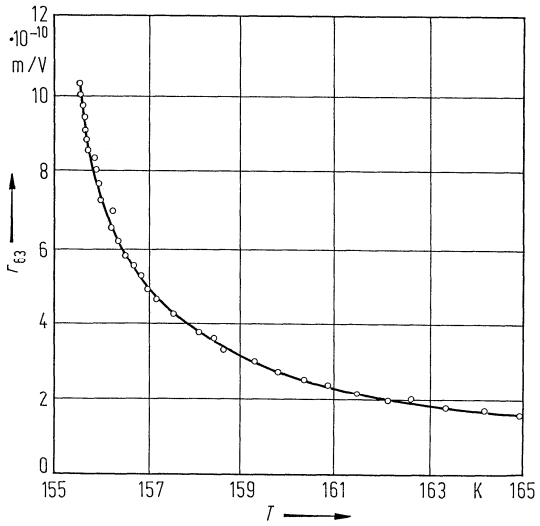

Fig. 33A-9-024. CsH_2AsO_4 (CDA). r_{63} vs. T [80Ani]. $\lambda = 632.8$ nm.

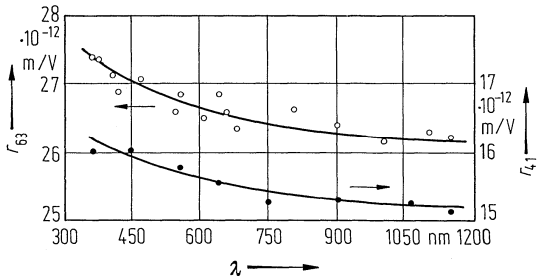

Fig. 33A-9-025. $CsH_{2(1-x)}D_{2x}AsO_4$ (x = 0.60). r_{63}, r_{41} vs. λ [80Vlo].

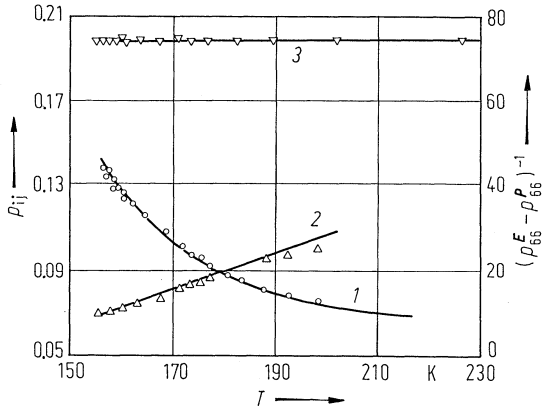

Fig. 33A-9-026. CsH_2AsO_4 (CDA). p_{ij}^{E}, $(p_{66}^{E} - p_{66}^{P})^{-1}$ vs. T [79Ani]. *1*: p_{66}^{E}. *2*: $(p_{66}^{E} - p_{66}^{P})^{-1}$. *3*: p_{31}^{E}. $\lambda = 632.8$ nm.

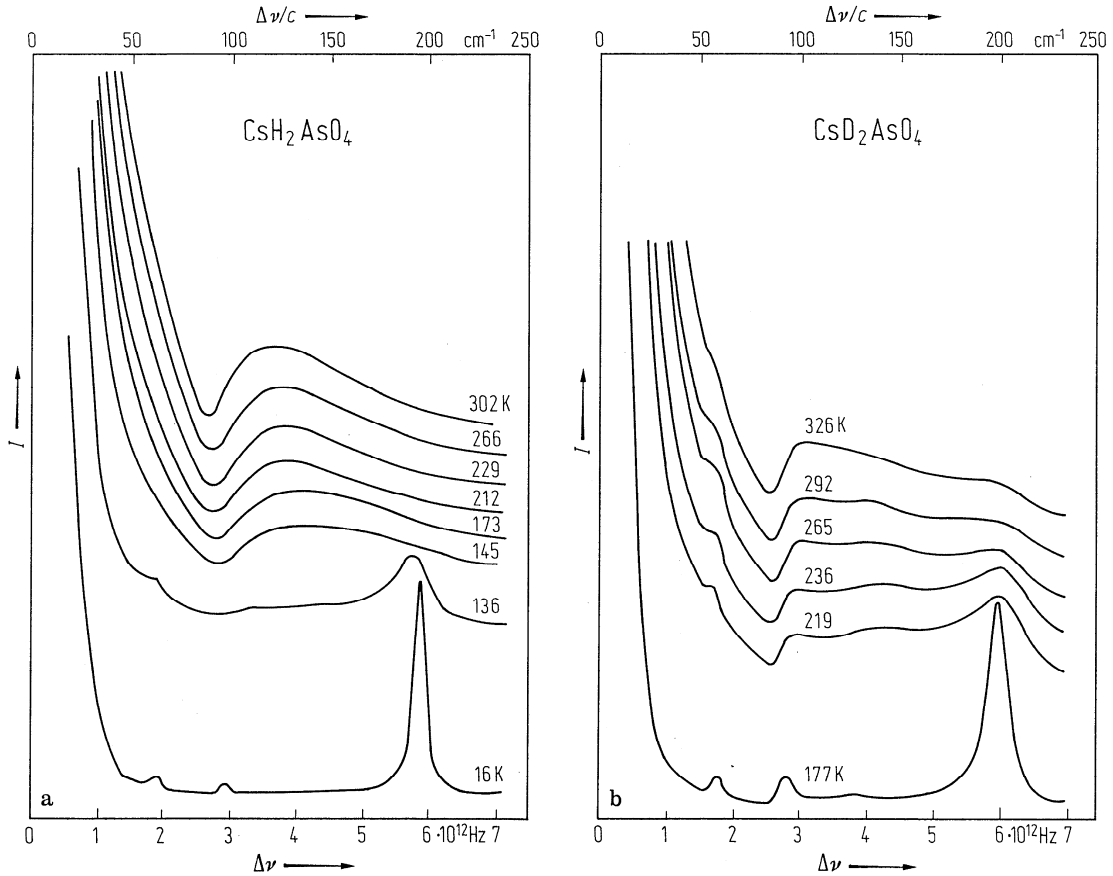

Fig. 33A-9-027. CsH_2AsO_4 (CDA), CsD_2AsO_4 (DCDA). I vs. $\Delta\nu$ [74Low]. (**a**) CDA. (**b**) DCDA. I: Raman scattering intensity of B_2 modes measured with scattering geometry $Y(XY)X$. Parameter: T.

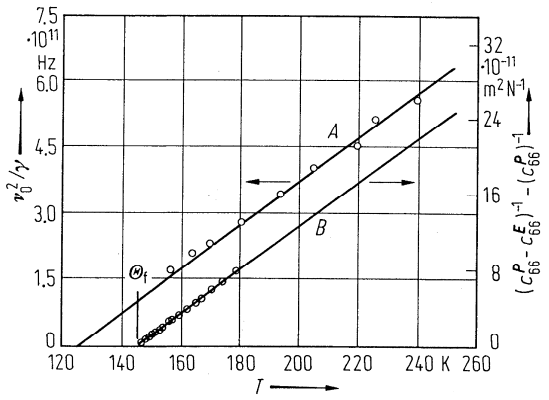

Fig. 33A-9-028. CsH_2AsO_4 (CDA). ν_0^2/γ vs. T and $(c_{66}^{\boldsymbol{P}} - c_{66}^{\boldsymbol{E}})^{-1} - (c_{66}^{\boldsymbol{P}})^{-1}$ vs. T [75Lag]. ν_0, γ: characteristic frequency and damping parameter of the ferroelectric soft mode deduced from Raman scattering spectra measured with a scattering geometry of $X(YX)Y$ (curve A). Curve B shows elastic constants obtained from Brillouin scattering.

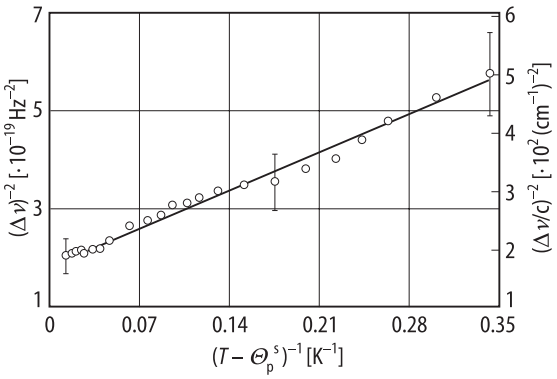

Fig. 33A-9-029. CsH_2AsO_4 (CDA). $(\Delta\nu)^{-2}$ vs. $(T - \Theta_p^s)^{-1}$ [77Azo]. $\Delta\nu$: frequency shift of Brillouin scattering. Θ_p^s : paraelectric Curie temperature for shorted crystal.

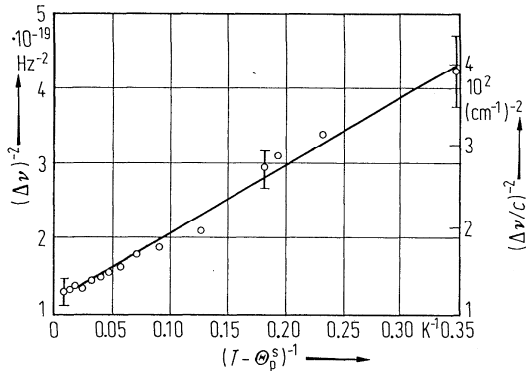

Fig. 33A-9-030. CsD_2AsO_4 (DCDA). $(\Delta\nu)^{-2}$ vs. $(T - \Theta_p^s)^{-1}$ [77Azo]. $\Delta\nu$: frequency shift of Brillouin scattering. Θ_p^s : paraelectric Curie temperature for shorted crystal.

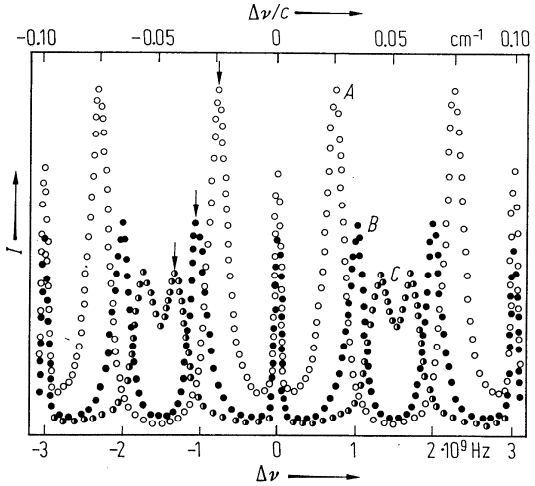

Fig. 33A-9-031. CsH_2AsO_4 (CDA). I vs. $\Delta\nu$ [75Lag]. I: intensity of Rayleigh and Brillouin scattering. $\Delta\nu$: frequency shift. Scattering geometry is $\overline{XZ}(X\overline{Z},Y)X\overline{Z}$. A: $T - \Theta_f = 0.05$ K, B: 0.85 K, C: 1.67 K. Arrows indicate the positions of the anti-Stokes Brillouin peaks of the order centered at zero.

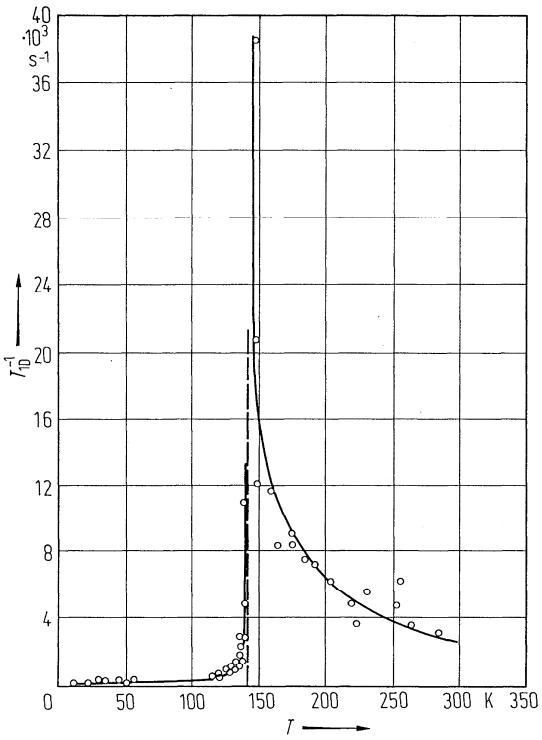

Fig. 33A-9-032. CsH_2AsO_4 (CDA). T_{1D}^{-1} vs. T [75Bli]. T_{1D}^{-1} : inverse of ^{75}As dipolar nuclear spin-lattice relaxation time.

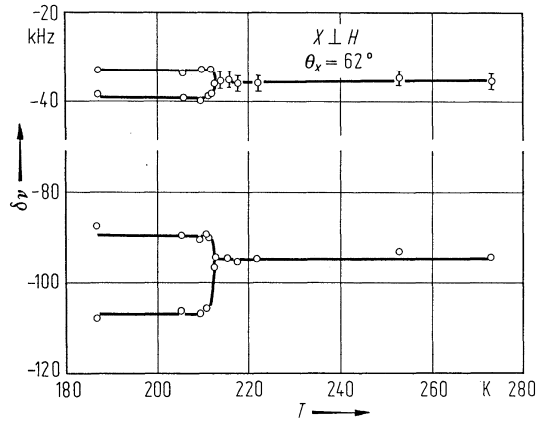

Fig. 33A-9-033. CsD_2AsO_4 (DCDA). $\delta\nu$ vs. T [71Bli]. $\delta\nu$: frequency difference between $m = 1 \rightarrow m = 0$ and $m = 0 \rightarrow m = -1$ transition of the deuteron, $\boldsymbol{H} \perp \boldsymbol{X}$, $\theta_x = 62°$, θ_x: angle between H and the crystal Y axis.

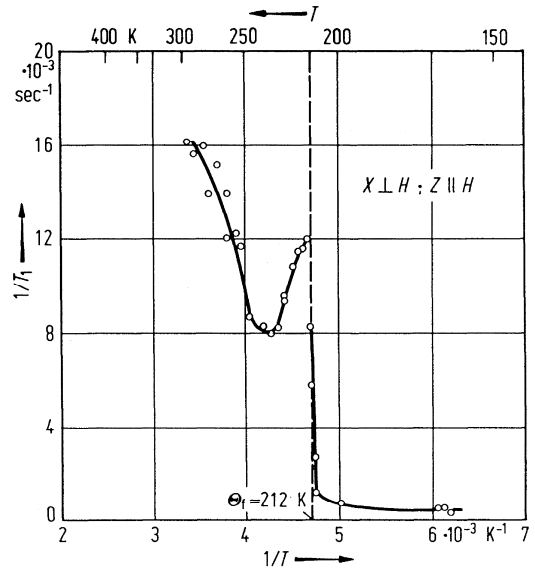

Fig. 33A-9-034. CsD_2AsO_4 (DCDA). $1/T_1$ vs. $1/T$ [71Bli]. T_1: spin-lattice relaxation time of deuteron, $\boldsymbol{X} \perp \boldsymbol{H}$, $\boldsymbol{Z} \parallel \boldsymbol{H}$. f = 10.5 MHz.

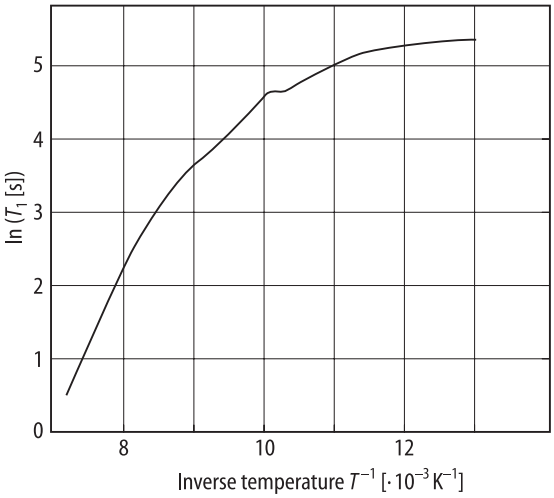

Fig. 33A-9-035. CsH_2AsO_4 (CDA). ln T_1 vs. T^{-1} [88Zhu]. T_1: spin-lattice relaxation time for ^{75}As from NQR measurements.

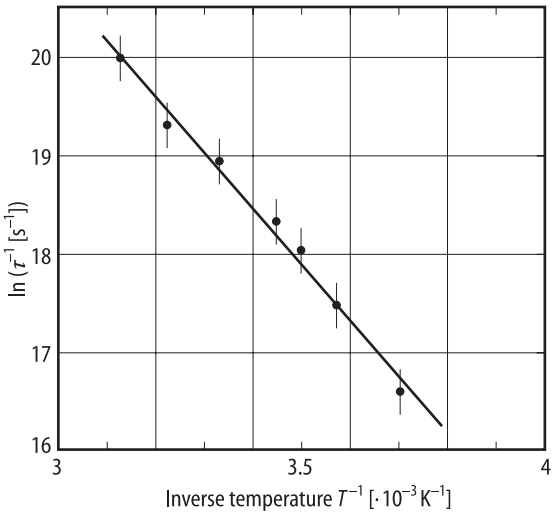

Fig. 33A-9-036. CsH_2AsO_4 (CDA). ln $(1/\tau)$ vs. T^{-1} [90Kah]. τ: correlation time [s] for AsO_4^{4-} obtained from ESR spectra.

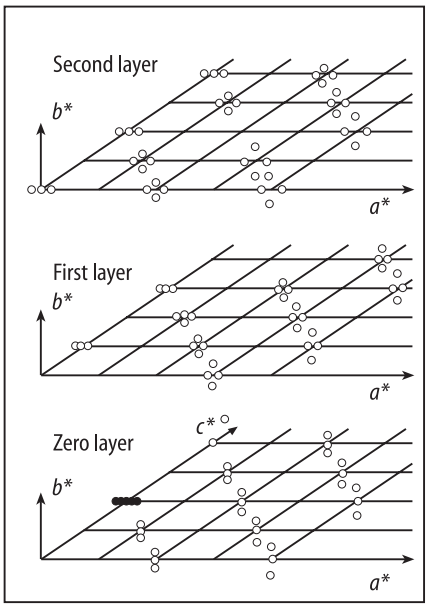

Fig. 33A-9-037. CsH_2AsO_4 (CDA). Domain splitting of neutron diffractions in (h0l) and parallel planes [76Mey2]. The Bragg points are split only in the a^*b^* plane. In addition the satellite positions at (002) are shown as full circles.

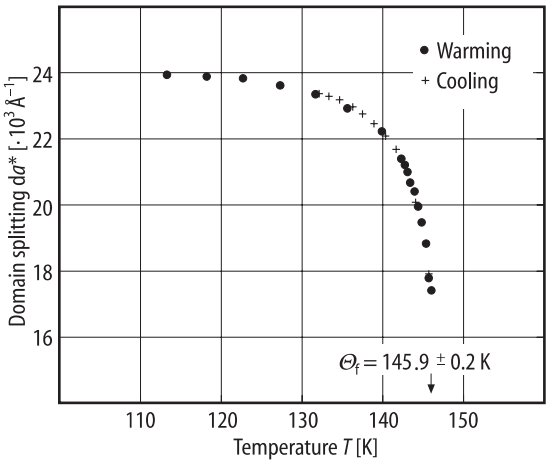

Fig. 33A-9-038. CsH_2AsO_4 (CDA). da^* vs. T [76Mey1]. da^*: domain splitting of neutron diffraction in the reciprocal space, d$a^* = a^* \tan x_y \approx 0.785 x_y$ where x_y is shear.

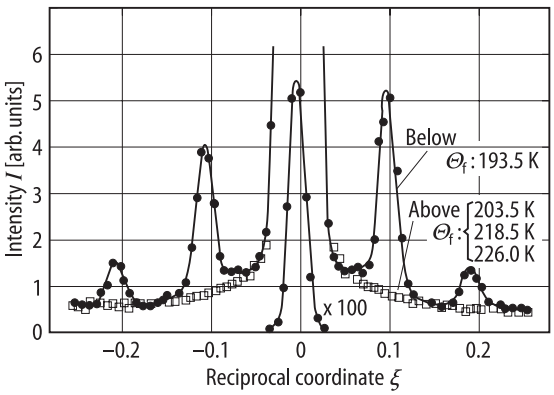

Fig. 33A-9-039. CsD_2AsO_4 (DCDA). I vs. ξ [74Die]. Parameter: T. I: intensity of neutron elastic scattering along the line (ξ 0 4).

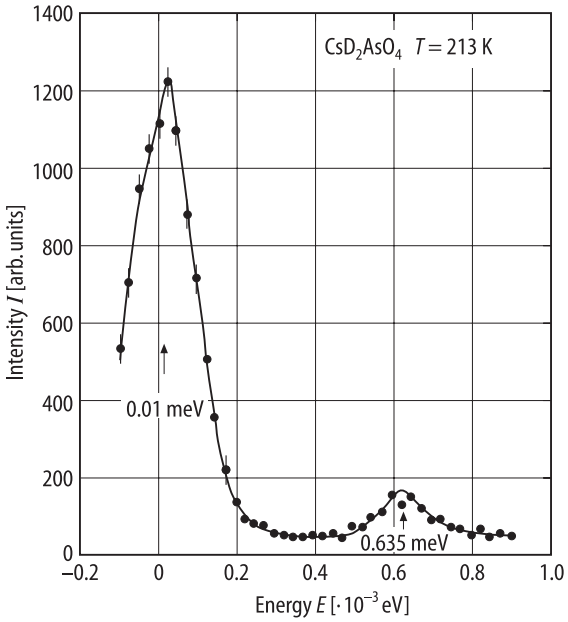

Fig. 33A-9-040. CsD_2AsO_4 (DCDA). I vs. E [76Mey1]. I: intensity of neutron inelastic scattering in the [001] zone at (2, 0.15, 0). $T = 213$ K.